A Wireless Microwave Telemetry Data Transfer Technique for Reciprocating and Rotating Components

Scott A. Miers
Argonne National Laboratory,
9700 South Cass Avenue,
Argonne, IL 60439

Glen L. Barna
IR Telemetrics, Inc.,
Houghton, MI 49931

Carl L. Anderson

Jason R. Blough

M. Koray Inal

Michigan Technological University,
Houghton, MI 49931

Stephen A. Ciatti
Argonne National Laboratory,
Argonne, IL 60439

Wireless microwave telemetry addresses the difficult issue of obtaining transducer outputs from reciprocating and rotating components through the use of advanced electronic components. This eliminates the requirements of a direct link between the transducer and the acquisition system. Accuracy of the transducer signal is maintained through the use of a double frequency modulation technique which provides temperature stability and a 20 point calibration of the complete system. Multiple transmitters can be used for larger applications and multiple antennas can be used to improve the signal strength and reduce the possibility of dropouts. Examples of automotive torque converter and piston temperature measurements are provided, showing the effectiveness of the wireless measuring technique. [DOI: 10.1115/1.2771562]

Keywords: telemetry, torque converter, piston temperature, data acquisition

Introduction

There is an increasing and inherent need to fully understand and measure mechanical systems as federal regulations tighten and consumer demands increase. This understanding begins with successful and efficient acquisition of data from devices such as automotive torque converters and internal combustion engines. The challenge lies in transferring the output from strategically placed transducers, such as pressure, strain, and/or temperature sensors, to suitable data acquisition systems. Continuous wires are not practical due to transducer locations deep within an engine or torque converter. Desired installations include internal combustion engine pistons, engine crankshafts, and automotive torque converters, as shown in Fig. 1 [1].

Two specific wireless microwave telemetry installations with corresponding data are presented, showing the wide range of applicability of the technique as well as the dynamic range and accuracy with which the original signal is reproduced.

Background

There have been several attempts at designing systems to record transducer outputs that are located in hard to reach areas [2–4]. Each has their advantages and disadvantages, as will be discussed in the following subsections.

Contact point or fusible plugs have been used in various forms for several years. Inserting a known material in a particular measurement location and subjecting the component to various temperatures, changes the hardness of the plug material, based on maximum temperature reached. While effective at capturing peak temperatures and being relatively inexpensive, dynamic phenomena are not able to be captured and nondestructive testing is impossible.

L-link systems [5] provide a continuous, solid connection to the transducer for reciprocating components, such as internal combustion engine pistons, connecting rods, and crankshafts. A schematic of a typical L-link system is shown in Fig. 2.

Modification of the existing hardware, i.e., engine, is extensive to accommodate the L-link mechanism, thus adding significant cost combined with increased imbalance in the system. Additionally, the transducer wires are continually flexed during operation and are susceptible to fatigue failure.

Both reciprocating and rotating components can utilize the slip ring configuration, which eliminates the continual flexing of transducer wires. Two similar material disks, one fixed and one rotating, are used to transfer the data from the transducer to the acquisition system. Continuous transducer data can be recorded with the slip ring configuration; however, contact noise can degrade the signal significantly and both size and cost can be an issue. Typically, the solution to noise reduction is expensive contact plates, which wear rather quickly.

Electromagnetic induction systems [6] transmit transducer output at a specified location in the cycle. Reciprocating components can benefit from inductive telemetry systems and are often installed to transmit piston temperatures at the bottom dead center location of the piston. While the system is relatively inexpensive and simple, only temperature measurements at bottom dead center are available. No information about component temperature near top dead center (i.e., the combustion event) is available.

Wireless telemetry addresses the shortfalls of the previous systems by providing the capability to measure transducer output continuously and eliminate any wire flexing. The telemetry transmitter is often located close to the transducer, so some additional weight is added to the dynamic system. However, this usually accounts for less than 10% of the total weight of the original system. Additionally, because there is no sliding or slipping connection, an additional noise source is eliminated.

This paper covers the study of wireless, microwave telemetry data acquisition, identification of its many advantages over existing measurement techniques, addresses its' few shortcomings, and presents current automotive torque converter and piston temperature data.

System Operation

The wireless telemetry system consists of four main components; the transmitter, the power supply, the antenna, and the receiver, as shown in Fig. 3 for a typical internal combustion engine piston installation.

The wireless telemetry component specifications are shown in Table 1. The 16 channels of input are typical and can be varied to accommodate the particular test being performed. Also note the

Submitted to ASME for publication in the JOURNAL OF ENGINEERING FOR GAS TURBINES AND POWER. Manuscript received October 9, 2006; final manuscript received May 23, 2007; published online February 21, 2008. Review conducted by Thomas W. Ryan III. Paper presented at the 2005 Fall Conference of the ASME Internal Combustion Engine Division (ICEF2005), Ottawa, Ontario, Canada, September 11–14, 2005.

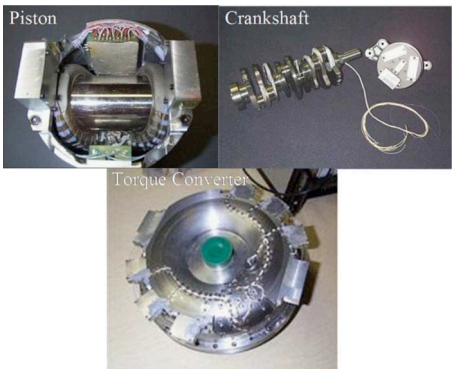

Fig. 1 Wireless telemetry installations

Table 1 Wireless telemetry specifications

Number of data channels per transmitter	16
Maximum bandwidth	10,000 Hz
Maximum operating temperature for electronics and batteries	150°C
Maximum internal loading	3,000 g reciprocating 50,000 g continuous
Transmitter weight	30–50 g
Multiplexing time	20–2000 ms
Acceptable inputs	Pressure, thermistors, strain, thermocouples, accelerometers, proximity
Battery weight	40 g

high level of internal loading able to be sustained by the electronics, thus making the system suitable for piston-type applications.

The transmitter is located in close proximity to the transducer and is responsible for acquiring the signals, multiplexing multiple transducer inputs, converting the low voltage input to a high-frequency signal, and for transmitting the signal to the antenna. Typical transmitter inputs are pressure, strain, and temperature transducers. Two frequency modulations (FMs) are utilized to produce a stable signal over a wide range of operating temperatures. A 16 channel sequential multiplexer exists inside the transmitter housing and controls which transducers signal is converted and transmitted to the antenna. The multiplexer can be designed to read the transducer input for as short a time as 20 ms or as long as 2 s.

The millivolt, emf output from the multiplexer is converted to a frequency-modulated, 10–50 kHz square wave in the first voltage to frequency conversion (V/F). Higher input voltage from the transducer is associated with higher frequencies in the square wave. This step produces a signal that contains the original transducer output, yet does not vary with changes in operating temperature, otherwise known as drift. The square wave is used to modulate a voltage-controlled oscillator (VCO) operating at a nominal frequency of 2.5 GHz. The output from the VCO, for example, could range from 2.49 GHz to 2.51 GHz. This frequency varying signal is transmitted to the environment and picked up by either single or multiple antennas. A schematic representation of the transducer output conversion process inside the transmitter is shown in the upper section of Fig. 4.

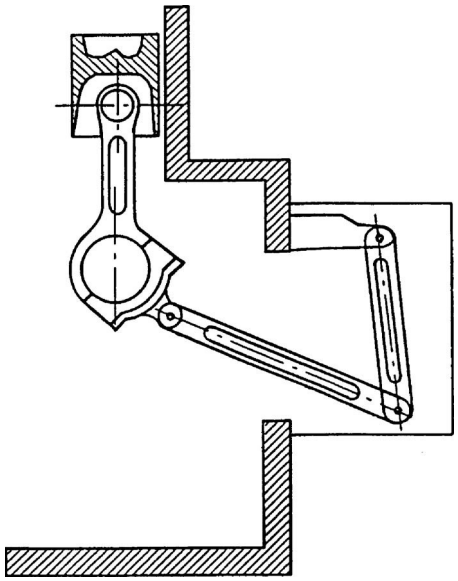

Fig. 2 Typical L-link system schematic

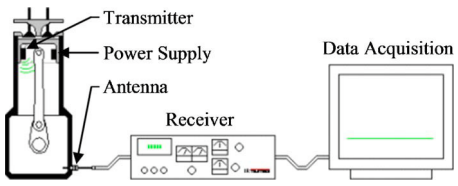

Fig. 3 Telemetry component schematic

The high-frequency signal from the transmitter is received by the antenna which can be installed up to 20 m from the transmitter output; however typical distances are less than 30 cm. The antenna signal is amplified and passes directly to the microwave receiver. The receiver is a superheterodyne unit that first down-converts the signal from 2.5 GHz to approximately 30 MHz. A frequency tuning knob is provided to match the incoming signal with the receiver specifications. Demodulation takes place to remove the 30 MHz signal and reproduce the square wave. A second demodulation reproduces the original transducer output, from the square wave, also known as the F/V section. Finally, the converted signal is output to a high-speed data acquisition system for analysis and post-processing. The lower half of Fig. 4 shows the schematic version of the two conversion steps within the receiver.

During the frequency to voltage conversion, it is possible for some of the square wave to bleed through and show up on the final voltage output of the receiver. Typically, this results in a 10–50 kHz ripple, superimposed on the reproduced transducer output. For this reason, a 2000 Hz, fifth-order, low-pass, Bessel filter is applied to the output of the F/V section, before high-speed acquisition. This also serves as an anti-aliasing filter. The effect of the low-pass filtering will be shown in the "Calibration" section.

There are two systems used to power the transmitter and multiplexer: batteries and inductive coils. Batteries are simple, easy to install, and provide 10–20 h of service when used with a thermal switch inside the transmitter. The g loading on batteries is limited to approximately 3000 rpm in engine applications, above which internal shorting of the battery is likely to occur. Inductive coils are not limited to g loading, but do require additional modifications to the original system. The inductive power unit is similar to an air-gap transformer with a stationary, externally powered coil and a moving coil. During some part of the cyclic operation, the coils couple and transmit power to the transmitter pack. Properly sized capacitors store the necessary power to operate the transmitter until the coils couple on the next cycle. Note that the transmitter and battery components are incorporated as a system to reduce the amount of imbalance to the original hardware.

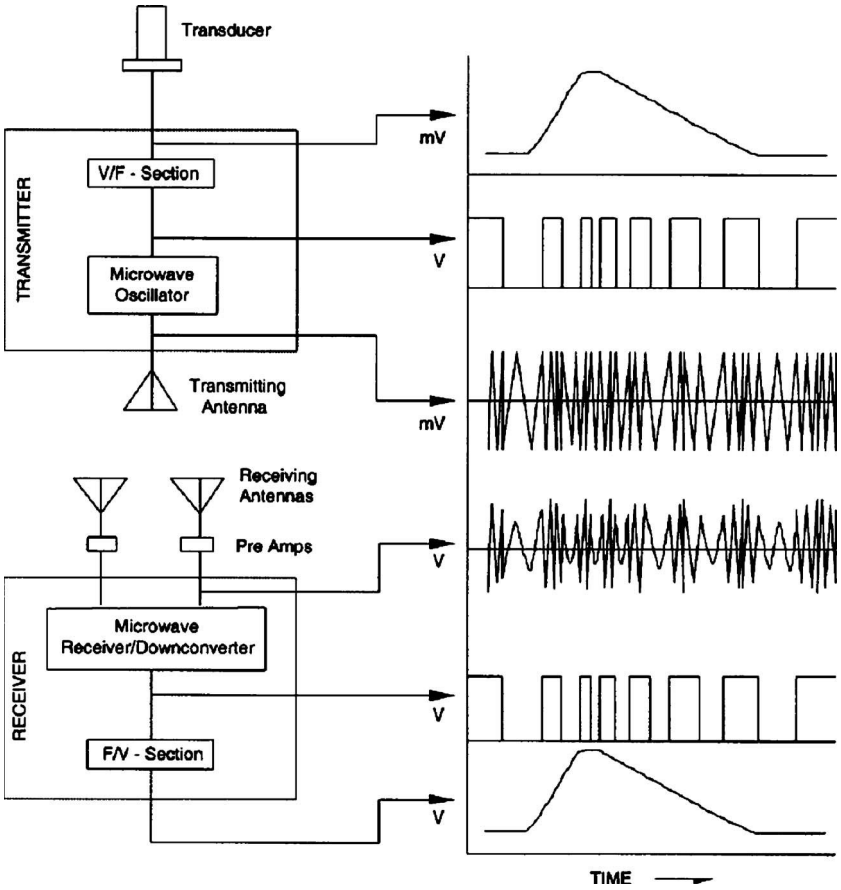

Fig. 4 Signal evolution, from transducer to output of receiver

Calibration

The calibration of the wireless telemetry consists of two separate operations. The first is a determination of the gain and phase of the overall system and the second is a 20 point temperature calibration and ice point verification.

Gain and Phase Determination. The gain and phase characteristics of the wireless telemetry system were obtained through the determination of the frequency response function. A 5–5000 Hz, millivolt burst-chirp signal was used to simulate a thermocouple output, over a wide range of dynamic temperature measurements. The signal was input to the telemetry system, in place of a thermocouple emf, and also input to a high-speed data acquisition system. The output of the telemetry receiver was input to a second channel of the data acquisition system, which allowed determination of the gain and phase characteristic. Connection details are shown in Fig. 5.

As shown in the upper part of Fig. 6, the cutoff frequency, based on 3 dB attenuation, was determined to be 2030.5 Hz. The phase remained linear up to 3500 Hz, as shown in the lower part of Fig. 6.

This is consistent with the fifth-order Bessel filter applied to the output of the last conversion step within the receiver. A 2000 Hz low-pass filter is used to eliminate the 10–50 kHz ripple associated with the frequency to voltage conversion. These results show

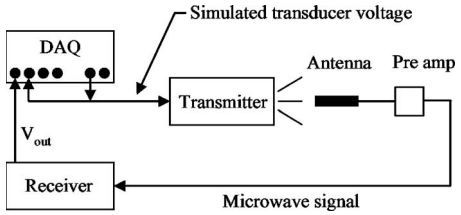

Fig. 5 Electrical connections for determining gain and phase characteristics

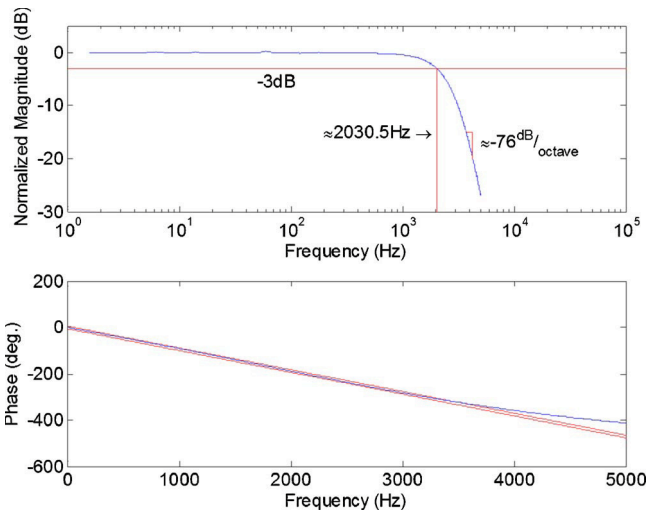

Fig. 6 Telemetry gain and phase characteristics

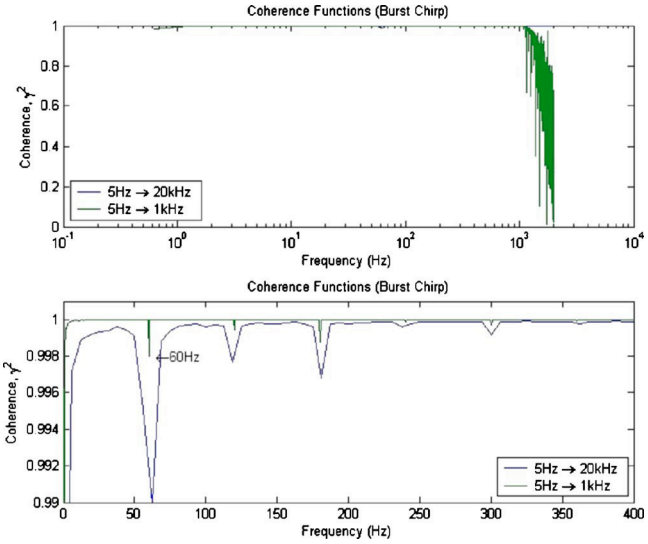

Fig. 7 Coherence function and 60 Hz noise

that the data being transmitted by the wireless telemetry system have not been significantly altered between the frequencies of 0 Hz and approximately 2000 Hz.

During the acquisition of data to determine the gain and phase characteristics, a 120 V ac, 60 Hz power cord was in close proximity to the antenna of the telemetry system. A coherence function calculation identified that the telemetry system recorded the 60 cycle noise and multiples up to 300 Hz, as shown in Fig. 7. Therefore, during an actual test, low-frequency (0–2000 Hz) noise sources should be kept away from the antenna area to avoid introducing noise into the transmitted signal. Also note that most engine noise sources, such as alternators, spark plugs, and coil drivers are well shielded from the transmitter pack due to the pack mounting location. Crankcase and torque converters are seldom large sources of noise and actually act as a shielded environment for the transmitter electronics and antennas.

20 Point Temperature Calibration. The wireless temperature transmitter is placed in Furnace No. 1 with one of its thermocouple inputs leading to an isothermal block in Furnace No. 2, as shown in Fig. 8. The transmitter temperature is monitored by calibrated thermocouple Meter A. During the first calibration test, the wireless transmitter is held at room temperature (20°C) while Furnace No. 2 is increased from room temperature to 350°C. The actual temperature of the transmitter input thermocouple is monitored with another thermocouple connected to calibrated thermocouple Meter B.

The transmitter output is recorded simultaneously with a temperature reading from calibrated thermocouple Meter B at approximately 20°C increments. The transmitter output versus temperature is plotted and a regression analysis technique is used to curve fit the data sets. The temperature of Furnace No. 1 (transmitter) is then increased to 135°C and Furnace No. 2 is operated from room temperature to 350°C, in 20°C increments. The elevated temperature environment data are compared to the room temperature output data and must agree to within 1%. This verifies the proper function of the transmitter electronic ice point. After the ice point function is verified, typically the 135°C calibration curve is used as the official calibration curve for service. If the operational temperature of the transmitter varies significantly from 135°C, then a new official calibration curve is created.

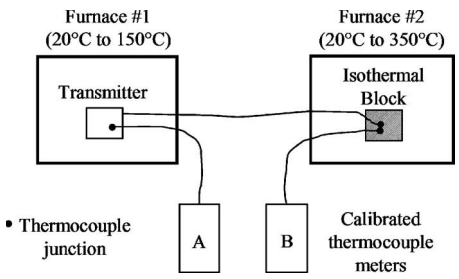

Fig. 8 Temperature calibration schematic

After the wireless transmitter and thermocouples have been installed on a component, such as a piston, the entire assembly is placed in Furnace No. 1 and heated to 150°C. The transmitter output is compared to calibrated thermocouple Meter A and to the official calibration equation. A minimum accuracy between the measured temperature and the actual temperature of 1% should be observed. Note that thermocouple accuracies are typically in the range of ±2%. After the transmitter has been used in an actual test, it is returned to the manufacturer for post-calibration to verify the absence of electronic drift or changes during the test. The post-calibration consists of repeating the two furnace tests outlined above and comparing this data to the original calibration curves.

Experimental Results

Two applications of the wireless microwave telemetry technique are briefly discussed in this section. Measurements of the fluid pressure on the stator blade of a rotating torque converter have been conducted to assist in the validation of computer simulations and promote further understanding of the fluid cavitation process. Additionally, high-speed diesel piston temperatures were recorded under a wide range of operating conditions to identify impingement signatures and provide boundary conditions for heat transfer analysis.

Automotive Torque Converters. Computational fluid dynamics (CFD) models of the torque converter operating in stall condition show that the lowest pressure in the converter typically occurs at the nose of the stator blade [7,8]. At stall condition fluid flows over the stator blade at a high angle of attack leading to flow separation on the suction side of the blade [9,10]. The combination of flow separation and high fluid velocities leads to very low pressures at the nose of the stator. Figure 9 is a cross section of the stator passage showing a CFD generated static pressure map at a location 25% of the way from the converter's outer shell to the converter's core (0.25 *S-C*) at a pump speed of 2000 rpm and a charge pressure of 70 psi.

An experimental stator was designed to measure static pressure at the nose of the stator, using wireless telemetry. Fifteen 0.5-mm-diameter pressure taps were situated in a 3×5 array that wrapped around the nose of the stator at locations shown in Fig. 10.

Each of the pressure manifolds were filled with automatic transmission fluid (ATF) throughout the pressure tap by letting air escape through an evacuation hole that was subsequently sealed with a gasket after all the air was evacuated. The microwave telemetry technique using a single transmitter mounted in the stator hub was used to transmit the 15 multiplexed transducer signals from the stator hub and out of the spinning torque converter. The sampling rate for the data was 12,800 Hz. Figure 11 is a photograph of the experimental stator with the cover removed showing the telemetry electronics mounted and potted in the hub of the stator.

Pressure data were taken at conditions that promoted the onset of cavitation. A cavitation signature was found in the fluctuating component of the static pressure, p'. Ca$'$ is a nondimensional fluctuating pressure that is referred to as the fluctuating cavitation number and is based on the mean square pressure (MSP) value of p', $\sqrt{\text{MSP}}$

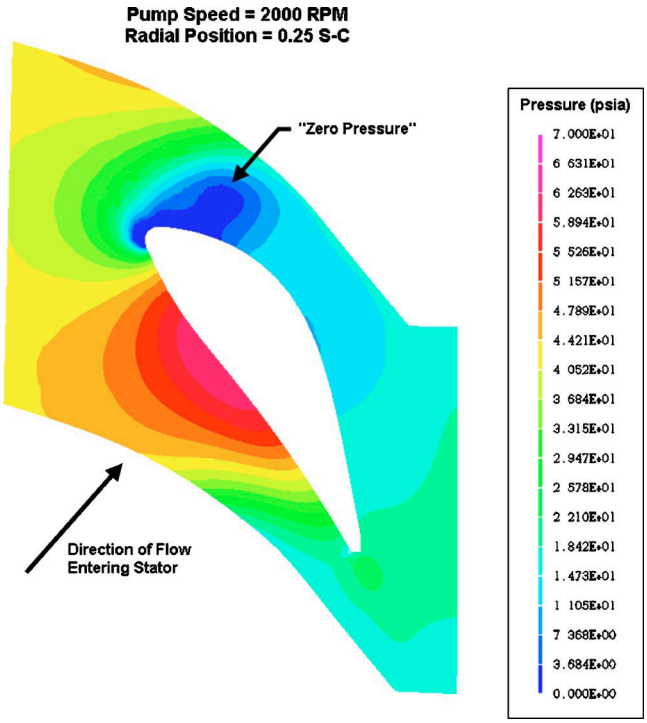

Fig. 9 CFD prediction of static pressures around a stator section at 0.25 *S-C*. The pump speed is 2000 rpm and the charge pressure is 70 psi.

Fig. 11 Stator with cover removed to show telemetry electronics installed in the hub

$$Ca' \equiv (\sqrt{\text{MSP}})/(1/2\rho(D\Omega)^2) \quad (1)$$

$\tilde{\Omega}_p$ is dimensionless pump speed defined as

$$\tilde{\Omega}_p \equiv (D\Omega)/(\sqrt{p_c/\rho}) \quad (2)$$

At a dimensionless pump speed of 1.25, cavitation bubbles start to form away from the blade and begin to damp the pressure fluctuations near the blade. When a dimensionless pump speed of 1.63 is reached, the fluctuating cavitation number is nearly zero and remains there for all higher values, as shown in Fig. 12. A dimensionless pump speed of 1.63 was defined as advanced cavitation and is the point were a three point running average was below 10% of the initial value of fluctuating cavitation number at low dimensionless pump speeds [11].

Ca′ dropped to a value near zero at the dimensionless pump speed marking advanced cavitation. This behavior is associated with a coalescence of the cavity formation zone near the surface where the pressure transducers were mounted. Attenuation of the pressure fluctuations by newly formed and growing cavities marks the inception of cavitation at the stator blades [11].

Piston Temperature Measurement Results. Two separate sets of analysis were performed with nearly the same set of data for the piston temperature measurements. The first was an impingement study on the surface of the piston and the second was a piston thermal loading study.

Figure 13 shows the location of the eight surface mounted thermocouples [1–6,14] and seven embedded thermocouples on a piston crosssection. Figure 14 shows the top view of the piston and corresponding thermocouple locations.

For the impingement study, the placement of the surface ther-

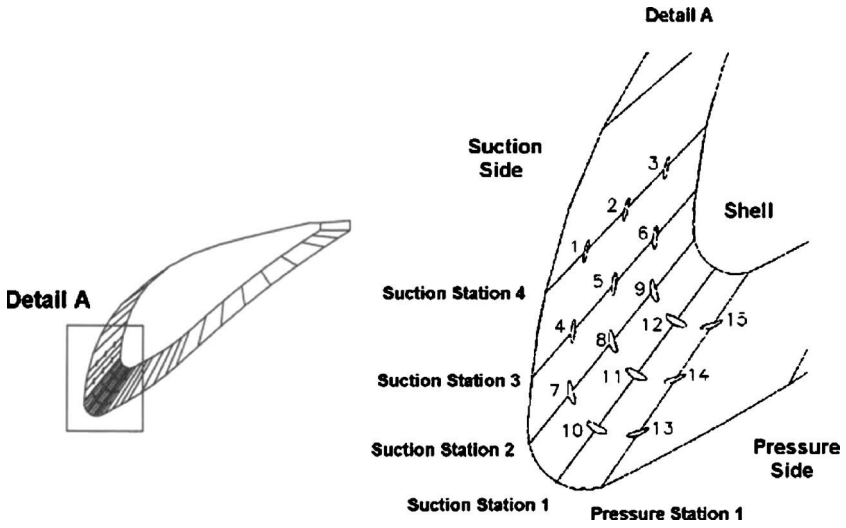

Fig. 10 Location of pressure taps on stator blade

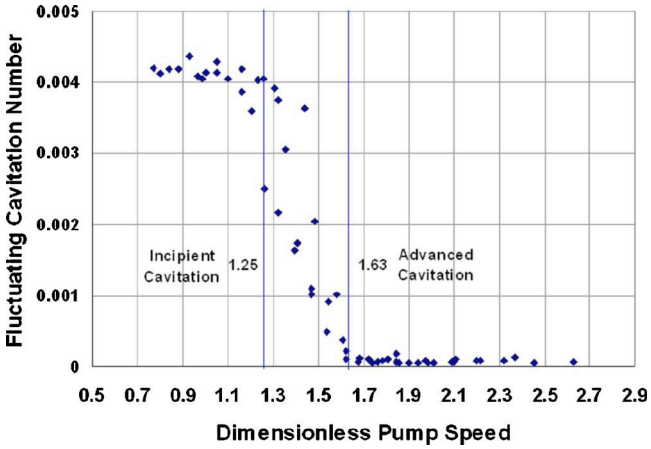

Fig. 12 Fluctuating cavitation number as a function of dimensionless pump speed at SS1, 0.25 S-C

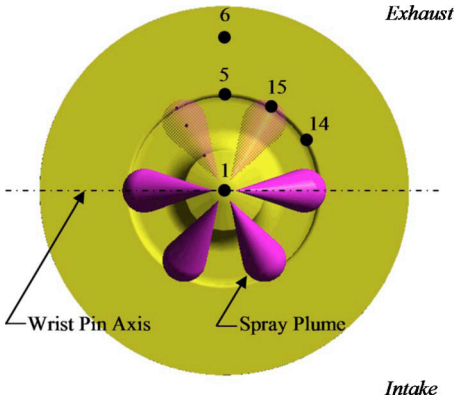

Fig. 14 Surface thermocouple locations from top view of piston (thermocouples 2, 3, and 4 omitted for clarity)

mocouples was chosen at locations on the piston of probable impingement. Thermocouples 5, 14, and 15 are mounted on the piston bowl lip and are circumferentially 30 deg from each other [14].

The fast-response surface thermocouples have an outer diameter of 1.55 mm (0.061 in.), a surface thermal deposition coating of 2 μm, and a time constant of 1 μs, according to the manufacturer (L. Jones, personal communication, March 20, 2002). Surface thermocouple specifications are provided in Table 2.

Figure 15 shows the surface temperature verses crank angle degree for the Thermocouple 5 location at two engine speeds, multiple loads, and 0 deg injector rotation.

0 crank angle degree (CAD) corresponds to the top dead center location of the piston. As load increases, both mean and peak surface temperature is observed to increase, as expected. When the same loads, speeds, and injector orientation are analyzed for Thermocouple 15, a unique signature appears at the higher loads, as shown in Fig. 16.

Thermocouple 15 displays a higher peak temperature and a distinct temperature profile around 0 CAD, compared to Thermocouple 5. Only Thermocouple 15 identified a distinct feature on the piston surface at this injector orientation. The locations on the piston and the operating condition of the engine are critical factors in determining if the signature is present. The change in the temperature profile is believed to be the result of the burning spray impinging on the thermocouple location. The temperature profile change occurs after the initial rise in the cylinder pressure which results from combustion, as shown in Fig. 17.

The rate of temperature change versus crank angle degree was calculated to further improve the identification of the impingement signature. Figure 18 shows the effectiveness of the identification technique. When impingement is present, it is transformed into a "spike" prior to top dead center, before the main combustion event. The peak value of the spike appears to correlate with the magnitude of the impingement event.

The speed/load dependence of the impingement signature was identified by calculating the peak value of $dT/d\theta$ at the impinge-

Table 2 Fast response surface thermocouple specifications

Thermocouple type	Triaxial, Type E (chromel/constantan)
Diameter	1.55 mm (0.061 in.)
Electrical connection	Surface deposited chromium
Connection thickness	2 μm
Time constant	Less than 1 μs
Bandwidth	10,000 Hz

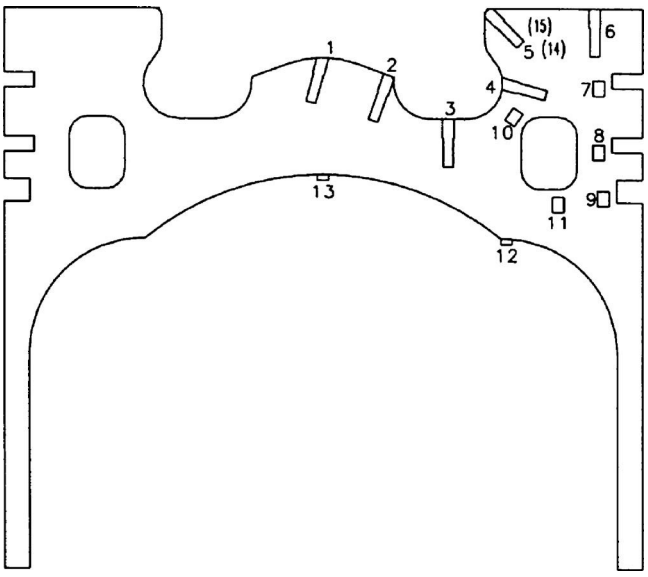

Fig. 13 Thermocouple locations on piston cross section

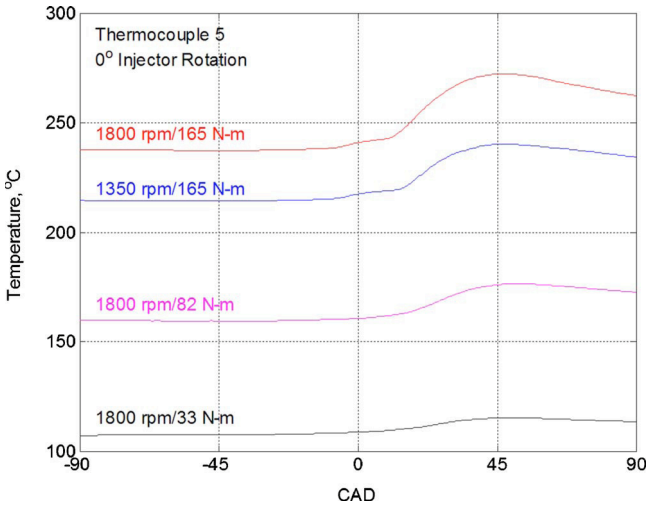

Fig. 15 Typical piston surface temperature traces: Thermocouple 5, 0 deg injector rotation

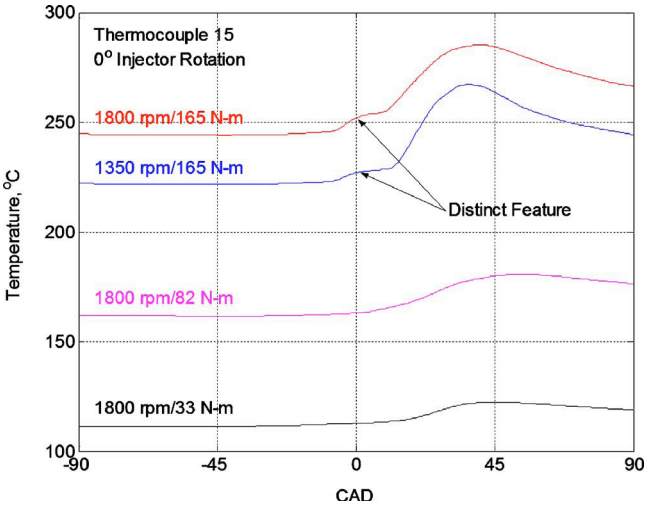

Fig. 16 Distinct feature in temperature trace: Thermocouple 15, 0 deg injector rotation

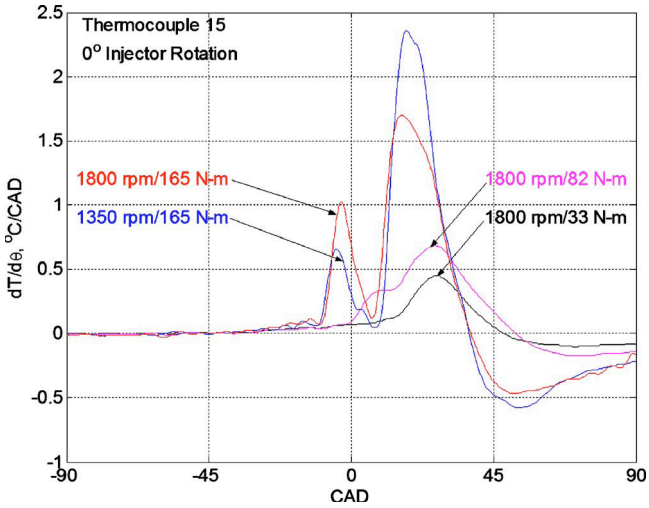

Fig. 18 $dT/d\theta$ identifies impingement at 1800rpm/165 N m and 1350 rpm/165 N m: Thermocouple 15, 0 deg injector rotation

ment location. The peak value of the impingement signature, relative to zero, was recorded for all test conditions. The smallest, measurable value of $dT/d\theta$ peak was 0.1. A threshold value of 0.15 was used to separate the data sets into impinging and nonimpinging conditions. Figure 19 shows a clear speed dependency between impinging and nonimpinging operating conditions [12].

The effect of impingement can be observed in the time domain and displays a unique signature at specific thermocouple locations, which do not exist at other locations on the piston surface. A simple parameter, $dT/d\theta$, effectively identifies the impingement event over a wide range of operating conditions and reveals a speed dependency on the impingement signature.

The instantaneous and steady-state piston thermal loading analysis involved the surface and the imbedded thermocouples to supply the boundary conditions for two-dimensional finite-element and one-dimensional semi-infinite solutions. Dynamic changes of temperature and heat flux exist several millimeters into the piston surface, with the highest temperatures observed at the surface [13]. A transient finite-element model was developed to solve for the temperature and heat transfer distribution throughout the piston cross section. The instantaneous surface heat transfer results from the finite-element model were then compared with the results from the one-dimensional semi-infinite solution. This was done to analyze the validity of one-dimensional semi-infinite behavior of the piston surface, a widely applied piston heat transfer assumption. A steady-state finite-element model, supplied with time-averaged temperature boundary conditions from the wireless telemetry, was also developed to calculate the distribution of heat transfer through different sections of the piston, such as the upper surface, rings, skirt, bottom of the piston, and oil gallery.

Two-dimensional (2D) effects are expected to be more dominant in locations such as the bowl lip compared to the center of the piston. The 1D and 2D results, as shown in Fig. 20 for the center of the piston [tc1], are almost identical. This proves that 2D effects at the center of the bowl do not significantly influence the heat transfer at this location.

However, a measurable difference in the heat transfer was observed for the piston bowl lip location [tc5] as shown in Fig. 21. The 1D semi-infinite solution overpredicts the peak heat flux to the piston lip for this particular case by approximately 14%.

One-dimensional semi-infinite heat transfer requires proper dissipation of the heat through the solid. In locations such as the bowl lip, heat transfer into the surface from both directions may cause the subsurface to reach higher steady periodic temperatures than the expected temperatures from the solution to the one-dimensional semi-infinite solid. Figure 22 shows the temperature

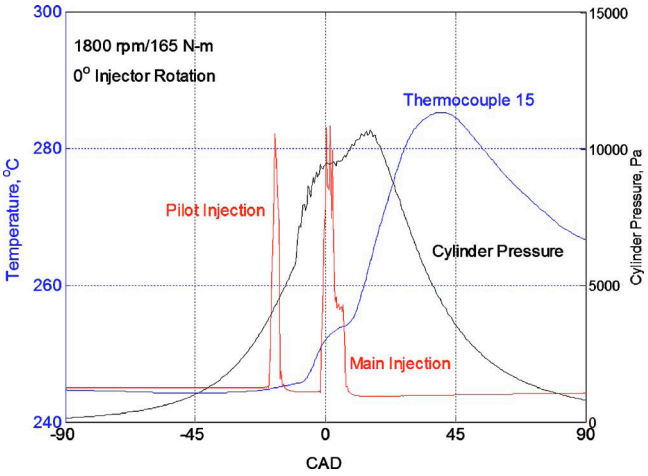

Fig. 17 Thermocouple 15, injection pulse and cylinder pressure relationship

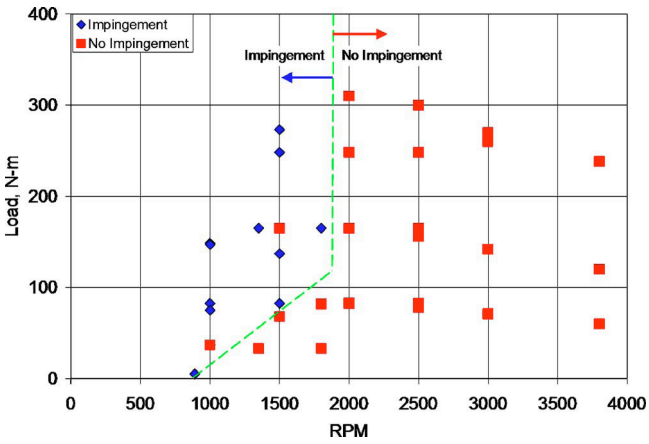

Fig. 19 Load versues rpm for impinging and nonimpinging conditions

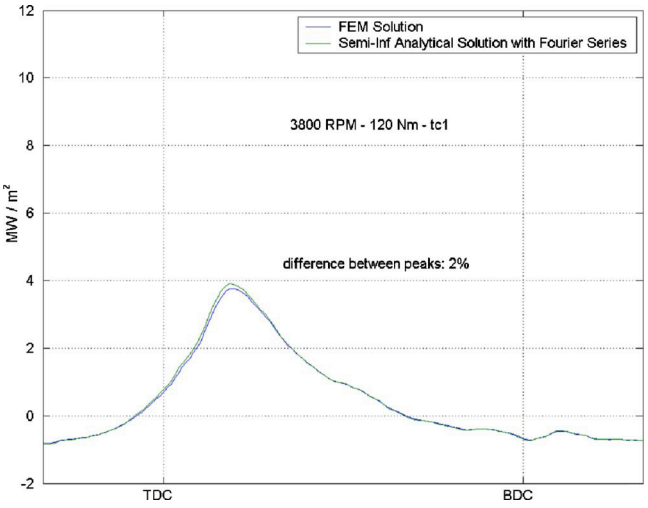

Fig. 20 Comparison of surface heat flux at thermocouple Location 1, for 2D FEM and 1D semi-infinite solutions

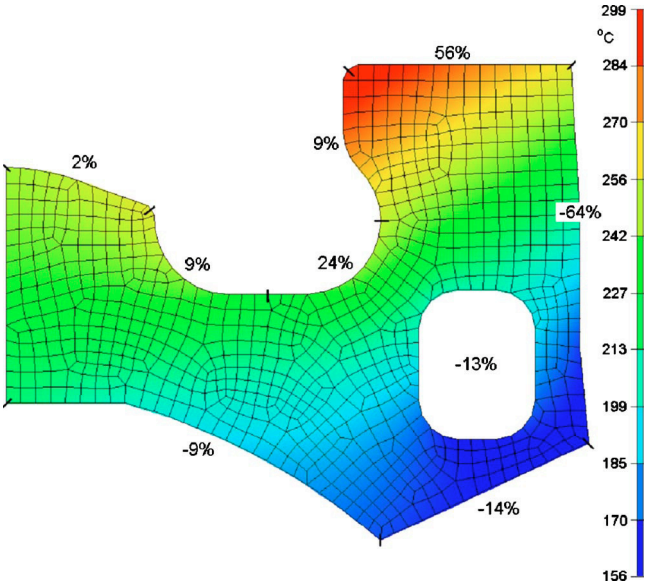

Fig. 22 Steady-state temperature and heat transfer (%) in a piston cross section

gradients from the steady-state, 2D, finite-element model and the distribution of the total steady-state heat transfer, in percent, at different sections of the piston.

Conclusions

1. The wireless microwave telemetry technique is an effective solution for measuring transducers in rotating and reciprocating components;
2. The high level of precision and accuracy with which measurements can be made in challenging locations has been demonstrated;
3. The wireless telemetry technique allows a continuous stream of data from the transducers, increasing component understanding; and
4. The system is extremely flexible for a variety of transducers, in a variety of applications, such as automotive torque converters and internal combustion engine pistons.

Acknowledgment

The submitted manuscript has been created by UChicago Argonne, LLC, Operator of Argonne National Laboratory ("Argonne"). Argonne, a U.S. Department of Energy Office of Science Laboratory, is operated under Contract No. DE-AC02-06CH11357. The U.S. Government retains for itself, and others acting on its behalf, a paidup nonexclusive, irrevocable worldwide license in said article to reproduce, prepare derivative works, distribute copies to the public, and perform publicly and display publicly, by or on behalf of the Government. Additional recognition is extended to Michigan Technological University and IR Telemetrics, Inc. for technical support and funding.

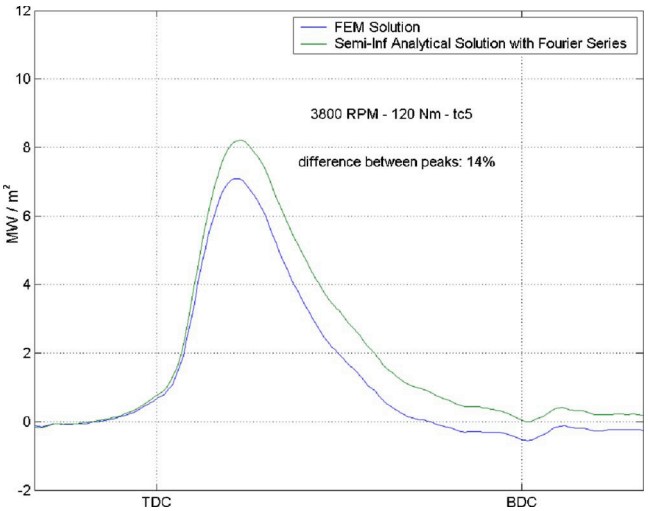

Fig. 21 Comparison of surface heat flux at thermocouple Location 5, for 2D FEM and 1D semi-infinite solutions

Nomenclature

ATF = automatic transmission fluid
CAD = crank angle degree
CFD = computational fluid dynamics
emf = electromotive force
FEM = finite-element method
FM = frequency modulation
F/V = frequency to voltage conversion
Hz = Hertz (cycles/s)
MSP = mean squared pressure
rpm = revolutions per minute
VCO = voltage controlled oscillator
V/F = voltage to frequency conversion

References

[1] Barna, G., 2004, IR Telemetrics, Inc.
[2] Lawrason, G., and Rollwitz, W., 1967, "A Temperature Telemetry Technique for Reciprocating Engines," SAE Technical Paper Series No. 670026, pp. 167–175.
[3] Burrahm, R. W., Davis, J. K., Perry, W. D., and De Los Santos, A., 1992, "Development of a Piston Temperature Telemetry System," SAE Technical Paper Series No. 920232, pp. 1–11.
[4] Barna, G., 1989, "An Infrared Telemetry Technique for Remote Piston Temperature Measurements in Internal Combustion Engines," M.S. thesis, Michigan Technological University, Houghton, MI.
[5] Assanis, D., and Friedmann, F., 1991, "A Telemetry Linkage System for Piston Temperature Measurements in a Diesel Engine," SAE Technical Paper Series No. 910299, pp. 1–12.
[6] Kato, N., Moritsugu, M., Shimura, T., and Matsui, J., 2001, "Piston Temperature Measuring Technology Using Electromagnetic Induction," SAE Technical Paper Series No. 2001-01-2027, pp. 1890–1896.
[7] Dong, Y., Dorivi, V., Attibele, P., and Yuan, Y., 2002, "Torque Converter CFD Engineering Part II: Performance Improvement through Core Leakage Flow and Cavitation Control," SAE Paper No. 020884.
[8] Schweitzer, J., and Gandham, J., 2002, "Computational Fluid Dynamics on Torque Converters—Validation and Application," *Proceedings 9th ISROMAC*.

[9] Ejiri, E., and Kubo, M., 1999, "Performance Analysis of Automotive Torque Converter Elements," ASME J. Fluids Eng., **121**, pp. 266–275.
[10] Watanabe, H., Kurshashi, T., and Kojima, M., 1997, "Flow Visualization and Measurement of Torque Converter Stator Blades Using a Laser Sheet Lighting Method and a Laser Doppler Velocimeter," SAE Paper No. 970680.
[11] Mekkes, J., Anderson, C., and Narain, A., 2004, "Static Pressure Measurements and Cavitation Signatures on the Nose of a Torque Converter's Stator Blades," Paper No. ISROMAC10-2004-035.
[12] Miers, S., 2004, "Impingement Identification and Characterization in a High Speed Diesel Engine using Piston Surface Temperature Measurements," Ph.D. dissertation, Michigan Technological University, Houghton, MI.
[13] Inal, M. K., 2005, "Thermal Loading and Surface Temperature Analysis of the Piston of a Small HSDI Diesel Engine," Ph.D. dissertation, Michigan Technological University, Houghton, MI.
[14] Miers, S., Anderson, C., Blough, J., and Inal, K., 2005, "Impingement Identification in a High Speed Diesel Engine using Piston Surface Temperature Measurements," SAE Trans. J. Mater. Manuf., **114–5**, pp. 845–851.